

1
2
3
4
5
6
7
8
9
10
11
12
13
14
15
16
17
18
19
20
21
22

Manuscript type: Full paper

**A method for subject-specific modelling and optimisation of the cushioning properties of
insole materials used in diabetic footwear**

Panagiotis E. Chatzistergos^{(1),*}, Roozbeh Naemi⁽¹⁾, Nachiappan Chockalingam⁽¹⁾

(1) CSHER, Faculty of Health Sciences, Staffordshire University, Stoke-on-Trent, United Kingdom.

(*) Corresponding author, **tel.:** +44 1782 295920

e-mail: panagiotis.chatzistergos@staffs.ac.uk, pchatzistergos@gmail.com

Keywords: Finite element, heel- pad, ultrasound indentation, inverse engineering, contact analysis, plantar pressure, plantar soft tissue, diabetic foot, hyperfoam

23 **Abstract:**

24 This study aims to develop a numerical method that can be used to investigate the cushioning properties of
25 different insole materials on a subject-specific basis.

26 Diabetic footwear and orthotic insoles play an important role for the reduction of plantar pressure in people
27 with diabetes (type-2). Despite that, little information exists about their optimum cushioning properties.

28 A new in-vivo measurement based computational procedure was developed which entails the generation
29 of 2D subject-specific finite element models of the heel pad based on ultrasound indentation. These
30 models are used to inverse engineer the material properties of the heel pad and simulate the contact
31 between plantar soft tissue and a flat insole. After its validation this modelling procedure was utilised to
32 investigate the importance of plantar soft tissue stiffness, thickness and loading for the correct selection of
33 insole material.

34 The results indicated that heel pad stiffness and thickness influence plantar pressure but not the optimum
35 insole properties. On the other hand loading appears to significantly influence the optimum insole material
36 properties. These results indicate that parameters that affect the loading of the plantar soft tissues such as
37 body mass or a person's level of physical activity should be carefully considered during insole material
38 selection.

39

40

41

42

43

44

45 **1. Introduction**

46 The diabetic foot disease is one of the most common complications of type-2 diabetes. Previous reports
47 highlight that approximately 15% of people with diabetes world-wide will at some stage develop diabetic
48 foot ulceration that could lead to amputation[1]. The complications of diabetes (type-2) are the most frequent
49 cause of non-traumatic lower-limb amputations[1]. While in the UK up to 100 people/week have a limb
50 amputated as a result of diabetes, it is indicated that up to 80% of these amputations could have been
51 prevented with correct management[2].

52 Even though it is clear that certain areas of the foot have a significantly higher risk for ulceration (i.e.
53 metatarsal head area, the heel and the hallux)[3] the mechanisms behind ulceration are not yet fully
54 understood. Foot ulcers in people with diabetes are multi-factorial and linked to a variety of clinical risk
55 factors, like peripheral neuropathy and vascular insufficiency[4], as well as biomechanical risk factors,
56 such as increased plantar pressure[3].

57 Previous in-vivo studies performed with age-matched groups of non-diabetic and diabetic volunteers have
58 found that diabetic plantar soft tissue tends to be thicker[5], stiffer[5,6], harder[7] and to return less energy
59 after a load/unload cycle (i.e. higher energy dissipation ratios)[8]. Moreover recent in-vivo results revealed
60 statistically significant correlations between the stiffness of the heel pad of people with diabetes (type-2) and
61 their blood sugar and triglycerides levels[9].

62 One of the most common experimental techniques used to study the in-vivo mechanical behaviour of plantar
63 soft tissues is ultrasound indentation. During the indentation test tissue deformation is measured from the
64 ultrasound images[5,8–10] and the applied force is measured from a load sensor enabling the calculation of
65 a force/deformation curve. This curve describes the macroscopic response of the plantar soft tissue to
66 loading and is influenced by the morphology of the tissue as well as by the size and shape of the indenter.
67 The effect of indenter size was numerically investigated by Spears et al.[11] to conclude that larger
68 indenters can produce more reliable and robust measurements compared to smaller ones.

69

70 In order to produce a more accurate and objective technique for the material characterisation of plantar soft
71 tissue Erdemir et al.[10] combined the in-vivo indentation test with finite element (FE) modelling.
72 Axisymmetric FE models of the indentation test were used to inverse engineer the values of the material
73 coefficients of a simplified hyperelastic bulk soft tissue.

74 One of the main therapeutic objectives for the management of the diabetic foot syndrome is the reduction of
75 plantar pressure. Although, therapeutic footwear and orthotic insoles play an important role in redistributing
76 the plantar load[12–15], very little information exists on the optimum cushioning properties of the materials
77 used as foot beds, insoles or a sole. Whilst the criteria for the selection of orthotic insole materials, which
78 were devised some time ago, identify stiffness[16] and the material's "pressure distributing properties"[17]
79 as critical factors for selection, no quantitative method exists to identify the most appropriate material on a
80 subject-specific basis[18,19]. As it stands there is no guideline about how "soft" or "stiff" an insole should
81 be. Despite that, currently there is a huge number of commercially available insole materials and new ones
82 are produced every year.

83 In this context the purpose of this study is to set the basis for an integrated procedure for the subject-specific
84 FE modelling of the heel pad upon which the investigation of the mechanical compatibility between heel
85 and insole would be possible. Such procedure would allow the optimal cushioning of the insole to be
86 determined based on subject-specific characteristics.

87

88 **2. Methods**

89 **2.1 Ultrasound indentation**

90 A healthy volunteer (age= 38 y, body mass= 82 Kg) was recruited for the purpose of this study. Ethical
91 approval was sought and granted by the University Ethics Committee and the subject provided full informed
92 consent.

93 An ultrasound indentation device (Figure 1) comprising an ultrasound probe connected in series with a
94 load cell (3kN, INSTRON) was utilised to perform indentation tests at the area of the apex of the
95 calcaneus[9]. The instrumented probe was mounted on a rigid metallic frame that is equipped with a
96 ball-screw linear actuator and a hand-wheel for the manual application of loading as well as with
97 adjustable foot supports to fix the subject's foot (Figure 1). A complete anti-clockwise revolution of the
98 hand wheel generates 5 mm of linear movement in the forward direction. During loading and unloading
99 the crank handle was rotated with a target shaft angular velocity of 90 deg/sec with the help of a
100 metronome. The actual deformation rate that is imposed by the device for this target angular velocity
101 had been previously measured during the pilot testing of the device to be equal to 0.96 mm/sec \pm 0.14
102 mm/sec[9]. This measurement was based on the results of heel indentation tests from 17 healthy
103 subjects[9].

104 The tests were performed using an 18 MHz linear array ultrasound probe (MyLab25, Esaote, Italy) which
105 is capable of imaging the entire width of the calcaneus. More specifically the footprint area of the
106 ultrasound probe was 3.5 cm² and its field-of-view was 42 mm wide and 40 mm deep. Before testing,
107 the subject's right foot was fixed on the device and the instrumented probe was carefully positioned to
108 image the medio-lateral (frontal) plane of the apex of the calcaneus (Figure 2A). The test's imaging
109 plane was identified from sequential ultrasound images of the heel at different planes[9]. During loading
110 the instrumented probe was pressed against the plantar side of the heel compressing the heel pad. More
111 specifically, the heel of the volunteer was subjected to five preconditioning load/unload cycles followed
112 by three measurement cycles to a maximum compressive force of 80 N. The applied force was recorded
113 using the load cell while the initial thickness and the deformation of the heel pad was measured after
114 the completion of the test from the ultrasound images (Figure 1) with the help of video analysis software
115 (Kinovea open source project, www.kinovea.org). Data were sampled at 28 Hz and utilised after the
116 completion of the tests to create an average force/deformation curve. After the completion of the loading
117 procedure and before releasing the subject's foot from its supports the width of the heel was also
118 measured using a digital calliper. The measurement was taken on the ultrasound imaging plane which

119 was identified using the ultrasound probe as a guide. The reproducibility of this simple measurement
120 was established through a test/ re-test procedure.

121 The magnitude of the applied load (i.e. 80 N) was decided based on preliminary barefoot plantar
122 pressure measurements. More specifically a pressure sensor (F-scan®, Tekscan, Boston, MA, US) was
123 used to measure the peak pressure of the entire heel area during quiet stance and then to calculate the
124 net compressive force that is applied to a section of the heel that is similar to the one imaged during the
125 indentation test. This section was defined around the location of peak pressure and its thickness was the
126 same as the ultrasound probe. Ten trials were performed in total where peak pressure and compressive
127 force were recorded for 15 sec with sampling frequency of 2 Hz. The average peak pressure and
128 compressive force were calculated for each trial.

129

130 2.2 Inverse engineering of the material coefficients of heel pad

131 The inverse engineering of the material coefficients of the plantar soft tissue entails the design of a subject-
132 specific FE model of the indentation test. More specifically the indentation test is simulated using a 2D
133 (plane stress with thickness) FE model comprising a rigid calcaneus and a bulk soft tissue. The geometry
134 of the model is reconstructed from an ultrasound image showing the heel pad under maximum
135 compression (Figure 2A). Using Matlab to outline the calcaneus (Figure 2B) a series of key-points is
136 defined and imported into the FE simulation software (ANSYS 12) to create the FE model of the
137 heel(Figure 2C). The thickness of the soft tissue in the FE model is modified to correspond to the initial
138 tissue thickness measured from the indentation test. The model's width was also uniformly expanded to
139 the value of the measured heel width (Figure 2C). The model of the heel was meshed with 4-node
140 quadrilateral elements (Plane182) using a free-mesh generator[20]. On the other hand the ultrasound
141 probe was simulated as a rigid trapezoid that is in frictionless contact with the plantar side of the soft
142 tissue (Figure 2C). The indentation procedure was simulated by fixing the probe and imposing a
143 displacement to the calcaneus equal to the maximum deformation measured experimentally. This
144 simulation enables the numerical estimation of the force/deformation curve for the indentation test.

145 The heel pad was simulated as nearly incompressible[21–23] Ogden hyperelastic (1st order) material.

146 The strain energy potential for this material model is defined as follows[20]:

$$147 \quad W = \frac{\mu_{tissue}}{\alpha_{tissue}} \left(\bar{\lambda}_1^{\alpha_{tissue}} + \bar{\lambda}_2^{\alpha_{tissue}} + \bar{\lambda}_3^{\alpha_{tissue}} - 3 \right) + \frac{1}{d_{tissue}} (J - 1)^2 \quad (1)$$

148 where $\bar{\lambda}_p^a$ ($p = 1, 2, 3$) are the deviatoric principal stretches, J is the determinant of the elastic
149 deformation gradient and μ_{tissue} , α_{tissue} and d_{tissue} are the material coefficients defining the mechanical
150 behaviour of the material. Coefficients μ_{tissue} and α_{tissue} are indirectly related to the material's initial
151 shear modulus and strain hardening/softening respectively while coefficient d_{tissue} is directly related
152 to the material's Poisson's ratio (ν). Assuming that the heel pad is nearly incompressible (i.e. $\nu=0.499$)
153 leaves only two material coefficients to be calculated (i.e. μ_{tissue} and α_{tissue}). For this purpose an opti-
154 mization algorithm was employed to find the values of μ_{tissue} and α_{tissue} that minimize the difference
155 between the numerical and the experimental force/deformation curves. Please also see supplementary
156 material for more information on the inverse engineering procedure (Supl.Mat.1).

157

158 2.3 Simulation of the contact between heel and insole material

159 The subject-specific model of the indentation test was modified to simulate the contact between the heel pad
160 and an insole material. More specifically the FE model of the rigid ultrasound probe was replaced by a layer
161 of a compliant foam material with uniform thickness of 10 mm (Figure 4A). The friction coefficient between
162 the heel pad and the insole material was set to 0.5[10]. The mechanical behaviour of the foam material was
163 simulated using the Ogden hyperelastic foam model (1st order). The strain energy potential for this
164 material model is defined as follows[20]:

$$165 \quad W = \frac{\mu_{foam}}{\alpha_{foam}} \left(J^{\alpha_{foam}/3} (\bar{\lambda}_1^{\alpha_{foam}} + \bar{\lambda}_2^{\alpha_{foam}} + \bar{\lambda}_3^{\alpha_{foam}}) - 3 \right) + \frac{\mu_{foam}}{\alpha_{foam} \beta_{foam}} (J^{-\alpha_{foam}} \beta_{foam} - 1) \quad (5)$$

166 where $\bar{\lambda}_p^{\alpha_{foam}}$ ($p = 1, 2, 3$) are the deviatoric principal stretches, J is the determinant of the elastic
167 deformation gradient and μ_{foam} , α_{foam} and β_{foam} are the material coefficients. Coefficients μ_{foam} and

168 α_{foam} are indirectly related to the material's initial shear modulus and strain hardening/softening
169 respectively while β_{foam} is directly related to the material's Poisson's ratio (ν).

170 The material coefficients of the foam material were initially assigned for commercially available PU foam
171 that is used in diabetic footwear. These values were not available from the manufacturer and were calculated
172 following a combined experimental and numerical approach as follows: $\mu_{\text{PU}}=39.6$ kPa, $\alpha_{\text{PU}}=19.3$, $\nu_{\text{PU}}=0.06$
173 (please also see supplementary material (Suppl.Mat.2)).

174 The aforementioned modelling procedure for the contact between the heel and an insole material was used
175 to give an insight in the optimum cushioning properties of flat insoles. The numerical calculations performed
176 to quantify the cushioning properties of an insole material were: the maximum deformation of the insole
177 material under constant load, the energy that is absorbed during loading, the peak plantar pressure and the
178 percent reduction of peak plantar pressure. Pressure reduction was calculated relatively to barefoot standing
179 on a rigid surface which was simulated by multiplying the μ_{foam} material coefficient of the PU foam by 10^6
180 to turn the simulated insole material into a practically rigid body. Quiet stance was simulated by fixing the
181 lower surface of the foam layer and applying a net compressive force of 80N at the calcaneus.

182

183 2.4 Validation

184 The accuracy of the predicted peak pressures between the heel pad and the insole material was assessed
185 through a testing procedure that closely matched the numerically simulated loading scenario (Figure 5). For
186 this purpose the ultrasound probe of the previously described ultrasound indentation device was replaced
187 with a rigid support for insole materials and the foot was loaded through a rectangular cuboid (120 mm \times 10
188 mm \times 10 mm) piece of the previously mentioned PU foam. A thin plantar pressure sensor (F-scan®,
189 Tekscan, Boston, MA, US) was also placed between the foot and the foam to measure peak pressure. The
190 subject's foot was subjected to five preconditioning load/unload cycles and three measuring ones to a
191 maximum compressive force of 80 N. During the last three load cycles the imposed force and the peak
192 plantar pressure between the foot and the PU foam were recorded at 28Hz. Both the loading rate and the

193 sampling rate used for this test were identical to those of the indentation tests. At the end the peak pressure
194 developed for 80 N of applied compression was averaged for the three trials and then compared with the
195 numerically calculated one.

196 An additional series of in-vivo measurements was performed to validate the ability of the subject-specific
197 FE model to predict the peak pressure reduction that is achieved by a foam material. For this purpose plantar
198 pressure measurements were performed with the subject standing (barefoot) on a 10 mm thick sheet of the
199 PU foam. Ten trials were performed in total and for each one of them the peak pressure of the entire heel
200 area was recorded for 15 sec. Considering the non-dynamic nature of loading a relatively low sampling
201 rate (2 Hz) was considered to adequately capture the plantar pressure during quiet stance. After
202 averaging, these results were compared to the ones recorded for the subject standing barefoot on a rigid
203 surface to calculate the percent pressure reduction achieved by the PU foam. At the end the
204 experimentally measured pressure reduction was compared to the numerically calculated one.

205

206 2.5 Parametric analyses

207 The aim of the first parametric investigation was to assess the sensitivity of the insole's cushioning properties
208 to its material coefficients μ_{foam} and α_{foam} . For this purpose 72 scenarios were simulated in total for twelve
209 different values of μ_{foam} ranging between $10 \text{ kPa} \leq \mu_{\text{foam}} \leq 210 \text{ kPa}$ (i.e. increments of 21 kPa) and six values
210 of α_{foam} between $2 \leq \alpha_{\text{foam}} \leq 12$ (i.e. increments of 2). The Poisson's ratio of the foam material was kept
211 constant ($\nu_{\text{foam}} = \nu_{\text{PU}}$).

212 The second parametric investigation aimed to assess the importance of subject-specific heel pad material
213 properties for the correct selection of insole material. Three scenarios were included in this investigation for
214 the cases of "average stiffness", "soft" and "stiff" heel pads. The case of "average stiffness" was simulated
215 using the material coefficients that were inverse engineered from the ultrasound indentation tests. The
216 remaining two cases were reconstructed based on literature by decreasing the values of the tissue's material

217 coefficients μ_{tissue} and α_{tissue} (Equation 1) by 50% or increasing them by 50% respectively to simulate a
218 “softer” or “stiffer” heel pad respectively[10].

219 The aim of the third parametric investigation was to assess the importance of subject-specific tissue thickness
220 for the correct selection of insole material. Three scenarios were included in this investigation, namely for a
221 heel pad of “average thickness” as well as for “thin” and “thick” heel pads. The last two cases were simulated
222 by decreasing or increasing the thickness of the heel pad respectively by 50% [5,10].

223 The aim of the last parametric investigation was to assess the importance of loading for defining the optimum
224 cushioning properties of insole materials. For this purpose the net force applied to the FE model was
225 increased from 80N to 160 N and 240 N (100% and 200% increase).

226 For each one of the aforementioned analyses the pressure reduction that can be achieved by foam materials
227 that exhibit different mechanical behaviour was assessed. The mechanical behaviour of the foam was
228 modified by changing the value of μ_{foam} ($10 \text{ kPa} \leq \mu_{\text{foam}} \leq 200 \text{ kPa}$) while α_{foam} and v_{foam} (Equation 5) were
229 kept constant. Initially coefficient α_{foam} was set equal to the optimum value found during the first parametric
230 investigation while v_{foam} was equal to v_{PU} . One higher and one lower value of α_{foam} were also included in the
231 investigation (increments of 2).

232

233 **3. Results**

234 **3.1 Ultrasound indentation**

235 The preliminary plantar pressure measurements showed that the average(\pm stdev) peak pressure for all
236 ten trials of barefoot standing on a rigid surface was equal to 176 kPa (\pm 7.6 kPa) while the average(\pm stdev)
237 net compressive force applied to a section of the heel that is similar to the one imaged during the
238 indentation test was 80N (\pm 4N).

239 The main output of the indentation test was the average force/deformation curve of the heel pad (Figure
240 3). The reconstructed outline of the calcaneus is shown in figure 2C while the thickness of the heel pad
241 and the width of the heel were measured to be 20.1 mm and 68 mm respectively.

242

243 3.2 Inverse engineering of the material coefficients of heel pad

244 The optimum solution for the inverse engineering procedure (Figure 3) was as follows:

245 $\mu_{\text{tissue}}= 1.18 \text{ kPa}$ and $\alpha_{\text{tissue}}= 17.38$.

246

247 3.3 Simulation of the contact between heel and insole material

248 The numerically estimated peak plantar pressure between the heel pad and the PU foam was 177 kPa (Figure
249 4C). The maximum deformation of the insole and the work that was absorbed during loading was 51.3%
250 and 0.182 Nm respectively. The respective peak pressure for the case of barefoot standing on a rigid surface
251 was 226 kPa (Figure 4B) which means that the predicted pressure reduction for the PU foam is 21.8%.

252

253 3.4 Validation

254 The average(\pm stdev) peak pressure that was measured for a testing procedure that closely matched the
255 simulations was 184 kPa (\pm 3kPa). The difference between the experimentally measured peak pressure and
256 the numerically estimated one was 3.8%.

257 The average(\pm stdev) peak pressure measured at the heel for barefoot standing on a 10 mm thick sheet of PU
258 foam was 137 kPa (\pm 10 kPa). Considering the value of the peak pressure for barefoot standing on a rigid
259 surface this measurement translates to 22.4 % peak pressure reduction compared to 21.8% that was predicted
260 from the FE analysis.

261 3.5 Parametric analyses

262 The sweep of the design space indicated that clear optimum values exist for the insole material coefficients.
263 Peak pressure was minimised for $\mu_{\text{foam}} = 52$ kPa and $\alpha_{\text{foam}} = 6$ and its minimum value was 166 kPa, which
264 corresponds to 26.5% reduction relatively to barefoot standing on a rigid surface (Figure 6A). On the other
265 hand the energy absorbed during loading was maximised for $\mu_{\text{foam}} = 31$ kPa and $\alpha_{\text{foam}} = 6$ (Figure 6B). The
266 maximum value of the absorbed energy during loading was 0.22 Nm. In contrast to peak pressure and
267 absorbed energy the maximum deformation appears to increase with decreasing μ_{foam} and α_{foam} for the entire
268 range of values that were tested (Figure 6C).

269 Reducing the values of the plantar soft tissue's material coefficients by 50% to produce a "softer" heel pad
270 caused a significant increase of barefoot peak pressure by 19%. On the contrary increasing the values of the
271 coefficients by 50% to simulate a "stiffer" heel pad caused a marginal increase of peak pressure by only 1%.

272 The maximum pressure reduction achieved for the case of a "softer" or "stiffer" heel pad was 28.4% and
273 32.4% respectively. In both cases maximum pressure reduction was achieved for $\alpha_{\text{foam}} = 6$ (Table 1). As it
274 can be seen in Figure 7A the insole material coefficients (μ_{foam}) that maximise pressure reduction for a "soft"
275 or a "stiff" heel pad appear to be the same as the ones found for a heel pad of "average stiffness". Similarly,
276 altered soft tissue properties appear to have no effect on the insole properties that maximise energy
277 absorption during loading (Figure 7B).

278 Changing the thickness of the heel pad had a significant effect on barefoot peak pressure. More specifically
279 decreasing heel pad thickness by 50% caused a 25% increase of peak pressure while increasing heel pad
280 thickness by 50% caused a 12% decrease of pressure.

281 Despite its effect on plantar pressure, heel pad thickness appeared to cause no change to the optimum insole
282 properties. The maximum pressure reduction that was found for the case of a "thin" or "thick" heel pad was
283 equal to 33.8% and 23.1% respectively. In both cases maximum reduction was again achieved for $\alpha_{\text{foam}} = 6$
284 (Table 1). As it can be seen in figures 7C and 7D the value of μ_{foam} that maximises pressure reduction and

285 energy absorbed for the cases of “thin” and “thick” heel pad appears to be the same as for a heel of “average
286 thickness”.

287 Increasing the net compressive force by 100% and 200% increased barefoot peak pressure by 105.7% and
288 227.6% respectively. In the case of 160 N (i.e. 100% force increase) a maximum pressure reduction of 26.1%
289 was achieved for $\mu_{\text{foam}} = 116$ kPa and $\alpha_{\text{foam}} = 6$ (Figure 7E). The maximum pressure reduction in the case of
290 240 N (i.e. 200% force increase) was 29.3% and it was achieved for $\mu_{\text{foam}} = 150$ kPa and $\alpha_{\text{foam}} = 6$ (Figure
291 7E). Moreover the maximum value of energy absorbed during loading (Figure 7F) for the cases of 160 N
292 and 240 N was 0.45 Nm and 0.68 Nm for $\mu_{\text{foam}} = 73$ kPa and $\mu_{\text{foam}} = 100$ kPa respectively ($\alpha_{\text{foam}} = 6$).

293

294 **4. Discussion**

295 Even though current literature is rich with elaborate geometrically detailed FE models of the entire
296 foot[21,22,24,25] and of the heel[26], the design and use of these models is labour intensive, computationally
297 expensive and requires a significant amount of information in terms of tissue geometry and mechanical
298 properties. This makes the extensive use of geometrically detailed FE models impractical for clinical
299 applications or the optimisation of footwear design. The use of anatomically focused simplified models has
300 been proposed as an alternative simulation approach to overcome the aforementioned problems associated
301 with geometrically detailed FE models[23,27].

302 In this context, the methodology presented here entails the creation of subject-specific 2D FE models of a
303 critical area of the heel based on relatively simple, non-invasive tests, namely ultrasound indentation and
304 plantar pressure measurements. The ultrasound indentation test provides the necessary information for the
305 design of the models and also for the inverse engineering of the material properties of the heel pad.

306 In a previous study, Erdemir et al.[10] also combined indentation tests with FE modelling to inverse engineer
307 the heel pad’s hyperelastic coefficients and reported the average initial shear modulus (K_0) of the heel pads
308 for twenty non-diabetic subjects to be equal to 16.54 kPa with a standard deviation of 8.27[10]. Similarly,
309 the initial shear modulus of the heel pad of the non-diabetic subject of the present study can be calculated as

310 follows: $K_0 = \frac{1}{2} \mu_{tissue} \alpha_{tissue} = 10.25 \text{ kPa}$ [20]. This value falls well within the range of values reported
311 by Erdemir et al.[10].

312 This modelling procedure was also employed for the simulation of the contact between the heel and insole
313 materials. As far as peak plantar pressure is concerned, the comparison between numerical and experimental
314 results for a single subject showed that the proposed technique can accurately predict the peak plantar
315 pressure for a loading scenario that closely matches the simulation, namely loading the heel using a strip of
316 foam material (Figure 5). Even though this loading is the closest one can get to the FE simulation, these two
317 loading scenarios are still not identical, mainly because of the shear stresses that are developed between the
318 loaded and unloaded tissues in the case of the in-vivo loading.

319 This first validation indicates that the proposed simulation technique can correctly solve the simplified
320 problem for which it was designed. Moreover comparing the results for the aforementioned idealised loading
321 scenario and quiet stance showed that the FE simulation overestimates the magnitude of peak pressure but
322 accurately estimates the normalised pressure reduction. More specifically the numerically estimated peak
323 pressure for the idealised loading scenario was 29.2 % higher than the one measured for quiet stance. On the
324 contrary the difference between the predicted and the measured pressure reduction was only 3.0 %.

325 All pressure measurements were performed using very thin (thickness \approx 0.25mm) sensors (F-scan®,
326 Tekscan, Boston, MA, US) that cannot offer any cushioning themselves and follow the curvature of the
327 insole. Based on that, the sensor's effect on the results was considered to be negligible and was not included
328 into the FE analysis.

329 After validation, the subject-specific model was utilised to assess the cushioning properties of different foam
330 materials. The results indicated that correct selection or fine-tuning of the mechanical behaviour of insole
331 materials can maximise an insole's capacity to reduce pressure and absorb energy during loading. Moreover
332 maximising the insole's capacity to reduce plantar pressure does not mean that its capacity to absorb energy
333 during loading is maximised too. Indeed it is indicated that an insole that is slightly "softer" than the one that
334 maximises pressure reduction is needed to maximise energy absorbed (Figure 6).

335 Previous in-vivo studies have found that the mechanical behaviour[5–8] and the thickness[5] of the plantar
336 soft tissue of people with diabetes change during the course of the disease. The importance of these
337 alterations for the assessment of ulceration risk has been highlighted by a series of numerical analyses which
338 indicate that these changes in mechanical properties and thickness of plantar soft tissues can lead to increased
339 plantar pressures[10,28,29]. Even though it is clear that people that have different risk for ulceration are
340 likely to need different types of footwear the exact implications of altered tissue mechanical properties and
341 thickness for the selection of insole material are not clear. In other words currently no guidelines exist to
342 inform health care professionals working on the diabetic foot if people with different plantar soft tissues
343 stiffness or thickness also need insoles made from different materials. The importance of the correct selection
344 of insole material has been previously highlighted by numerical studies indicating that the pressure-relieving
345 capabilities of footwear[15,30] as well as perceived comfort[25] are significantly influenced by the
346 mechanical properties of the insole material.

347 In this context the results of this study indicated that even though heel pad
348 mechanical properties and thickness influence plantar pressure they do not affect the optimum cushioning
349 properties of insole materials. Indeed as it can be seen in figures 7A-D the insole material properties that
350 maximise pressure reduction and energy absorbed during loading remain the same regardless of changes in
351 terms of tissue stiffness or thickness. Therefore it can be concluded that these two parameters are not likely
352 to be critical to inform insole material selection. In contrast to subject-specific tissue stiffness and thickness,
353 subject-specific loading appears to significantly influence the optimum insole material properties (Figures
354 7E,F).

355 Considering the plantar area of the FE model of the heel pad the three load magnitudes (i.e. 80 N, 160 N,
356 240 N) that were included in the study correspond to average pressures of 147 kPa, 294 kPa and 441 kPa
357 respectively. These values might be relatively high for static loading scenarios and more likely to be
358 developed during dynamic ones such as walking[31] or running[32], but the simulation revealed a clear
359 trend, indicating that the optimum stiffness of an insole material increased with loading. Even though more
360 testing is needed to confirm these results for dynamic loading the findings of this study indicate that the
361 cushioning properties of insole materials could possibly be optimised on a subject-specific basis using simple

362 information on loading and the factors that influence it (e.g. body mass, a person's type of weight-bearing
363 physical activity etc.).

364 Moreover further tests involving people with diabetes are also needed to see if a material selection method
365 that is based on loading could also be used to inform the prescription of diabetic footwear. At this point it
366 should be stressed out that the correct selection of materials is only one aspect of footwear that could be
367 optimised on a patient-specific basis. The overall structure of the footwear[33–35] as well as the degree of
368 congruity between the footwear and the foot[28] need also to be considered to maximise the efficiency of
369 diabetic footwear.

370 Because of the manual operation of the indentation device and limitations in the achievable loading rates the
371 modelling procedure presented here was limited to quasi-static loading scenarios and therefore the viscosity
372 of the plantar soft tissue was not taken into account. Besides that, it is clear from literature that the viscosity
373 can significantly alter the plantar soft tissue's response to dynamic loading and therefore it should be
374 considered in the case of dynamic loading[26,34,36–38].

375 Another limitation of this modelling procedure is that the use of a 2D model restricts its application to loading
376 scenarios that don't involve considerable out of plane loads. As a result of that the effect of plantar shear
377 stresses, which according to literature are altered in diabetic neuropathic patients and play an important role
378 for ulceration[39,40], cannot be investigated with the existing 2D FE models. On the other hand, the use of
379 a 2D model substantially reduced the computational power that is needed to perform each analysis and
380 enabled its use for the inverse engineering of the heel pad's material coefficients, which is a highly iterative
381 process. In addition, the use of a 2D model significantly simplified the reconstruction of the heel pad's
382 geometry and enabled the design of subject-specific models without the need for CT or MRI scans which
383 are costly and their analysis is very labour intensive. At this point it should be stressed out that the geometry
384 of the calcaneus is expected to influence the results of the analysis and reconstructing it for every subject
385 significantly enhances the subject-specificity of the analysis.

386 Moreover the assumption that the plantar soft tissue is a uniform bulk material means that this model cannot
387 be used to study the internal stress and strain fields of the tissue. The simplified simulation of the tissue's

388 internal structure could also compromise the reliability of the model for loading cases other than the ones
389 for which it was validated.

390 On the other hand the proposed modelling procedure was proven to be satisfactory accurate for the
391 simulation of heel pad's macroscopic response to quasi static loading and the analysis of the contact
392 conditions between the heel pad and different insole materials. This ability enabled a thorough investigation
393 of some important parameters that could affect the mechanical compatibility between the heel pad and insole
394 materials and shed new light on the optimum cushioning properties of insoles without the limitations of
395 commercially available materials. Moreover, the FE modelling procedure presented here offers an improved
396 approach for the inverse engineering of the heel pad's hyperelastic coefficients[10] which takes into account
397 the subject specific geometry of the calcaneus. In the future the method presented here could also be used
398 for other areas of the foot such as the metatarsal heads or the Hallux.

399

400

401 **Competing interests:** None declared

402

403 **Funding:** This work is supported through the project titled DiabSmart funded by the European
404 Commission (Grant Agreement Number 285985, Industry Academia partnerships and Pathways (FP7-
405 PEOPLE-2011-IAPP)).

406

407 **Ethical approval:** Ethical approval was sought and granted by the Staffordshire University Ethics
408 Committee.

409

410

411

412

413 **References**

- 414 [1] Boulton a J. The diabetic foot: a global view. *Diabetes Metab Res Rev* 2000;16 Suppl 1:S2–5.
- 415 [2] Diabetes UK. *Diabetes in the UK 2011– 12 Key Statistics on diabetes*. 2011.
- 416 [3] Ledoux WR, Shofer JB, Cowley MS, Ahroni JH, Cohen V, Boyko EJ. Diabetic foot ulcer
417 incidence in relation to plantar pressure magnitude and measurement location. *J Diabetes*
418 *Complications* 2013;27:621–6.
- 419 [4] Crawford F, Inkster M, Kleijnen J, Fahey T. Predicting foot ulcers in patients with diabetes: a
420 systematic review and meta-analysis. *QJM* 2007;100:65–86.
- 421 [5] Chao CYL, Zheng Y-P, Cheing GL-Y. Epidermal thickness and biomechanical properties of
422 plantar tissues in diabetic foot.pdf. *Ultrasound Med Biol* 2011;37:1029–38.
- 423 [6] Klaesner JW, Hastings MK, Zou D, Lewis C, Mueller MJ. Plantar tissue stiffness in patients
424 with diabetes mellitus and peripheral neuropathy. *Arch Phys Med Rehabil* 2002;83:1796–801.
- 425 [7] Piaggese A, Romanelli M, Schipani E, Campi F, Magliaro A, Baccetti F, et al. Hardness of
426 Plantar Skin in Diabetic Neuropathic Feet. *J Diabetes Complications* 1999;13:129–34.
- 427 [8] Hsu TC, Wang CL, Shau YW, Tang FT, Li KL, Chen CY. Altered heel-pad mechanical
428 properties in patients with Type 2 diabetes mellitus. *Diabet Med* 2000;17:854–9.
- 429 [9] Chatzistergos PE, Naemi R, Sundar L, Ramachandran A, Chockalingam N. The relationship
430 between the mechanical properties of heel-pad and common clinical measures associated with
431 foot ulcers in patients with diabetes. *J Diabetes Complications* 2014:(in – press).
- 432 [10] Erdemir A, Viveiros ML, Ulbrecht JS, Cavanagh PR. An inverse finite-element model of heel-
433 pad indentation. *J Biomech* 2006;39:1279–86.
- 434 [11] Spears IR, Miller-Young JE. The effect of heel-pad thickness and loading protocol on
435 measured heel-pad stiffness and a standardized protocol for inter-subject comparability. *Clin*
436 *Biomech (Bristol, Avon)* 2006;21:204–12.
- 437 [12] Reiber GE. Who is at risk of limb loss and what to do about it? *J Rehabil Res Dev*
438 1994;31:357–62.
- 439 [13] Ragnarson Tennvall G, Apelqvist J. Prevention of diabetes-related foot ulcers and
440 amputations: a cost-utility analysis based on Markov model simulations. *Diabetologia*
441 2001;44:2077–87.
- 442 [14] Healy A, Naemi R, Chockalingam N. The effectiveness of footwear as an intervention to
443 prevent or to reduce biomechanical risk factors associated with diabetic foot ulceration: A
444 systematic review. *J Diabetes Complications* 2013;27:391–400.
- 445 [15] Cheung JT-M, Zhang M. Parametric design of pressure-relieving foot orthosis using statistics-
446 based finite element method. *Med Eng Phys* 2008;30:269–77.
- 447 [16] Shurr D., Cook TM. *Methods, materials, and mechanics. Prosthetics Orthot., Prentice Hall;*
448 1990, p. 17–29.

- 449 [17] Campbell GJ, McLure M, Newell EN. Compressive behavior after simulated service
450 conditions of some foamed materials intended as orthotic shoe insoles. *J Rehabil Res Dev*
451 1984;21:57–65.
- 452 [18] Healy A, Dunning DN, Chockalingam N. Materials used for footwear orthoses: a review.
453 *Footwear Sci* 2010;2:93–110.
- 454 [19] Paton JS, Stenhouse E, Bruce G, Jones R. A longitudinal investigation into the functional and
455 physical durability of insoles used for the preventive management of neuropathic diabetic feet.
456 *J Am Podiatr Med Assoc* n.d.;104:50–7.
- 457 [20] ANSYS. ANSYS Release 12 Documentation. Canonsburg, PA, USA: ANSYS Inc; n.d.
- 458 [21] Guiotto A, Sawacha Z, Guarneri G, Avogaro A, Cobelli C. 3D finite element model of the
459 diabetic neuropathic foot: A gait analysis driven approach. *J Biomech* 2014:1–8.
- 460 [22] Isvilanonda V, Dengler E, Iaquinto JM, Sangeorzan BJ, Ledoux WR. Finite element analysis
461 of the foot: model validation and comparison between two common treatments of the clawed
462 hallux deformity. *Clin Biomech (Bristol, Avon)* 2012;27:837–44.
- 463 [23] Spirka T a., Erdemir A, Ewers Spaulding S, Yamane A, Telfer S, Cavanagh PR. Simple finite
464 element models for use in the design of therapeutic footwear. *J Biomech* 2014.
- 465 [24] Chen W-M, Lee T, Lee PV-S, Lee JW, Lee S-J. Effects of internal stress concentrations in
466 plantar soft-tissue--A preliminary three-dimensional finite element analysis. *Med Eng Phys*
467 2010;32:324–31.
- 468 [25] Franciosa P, Gerbino S, Lanzotti A, Silvestri L. Improving comfort of shoe sole through
469 experiments based on CAD-FEM modeling. *Med Eng Phys* 2013;35:36–46.
- 470 [26] Fontanella CG, Wilhjelm JE, Virga a., Carniel EL, Matteoli S, Corvi a., et al. Investigation on
471 the load-displacement curves of a human healthy heel pad: In vivo compression data compared
472 to numerical results. *Med Eng Phys* 2012;34:1253–9.
- 473 [27] Yarnitzky G, Yizhar Z, Gefen A. Real-time subject-specific monitoring of internal
474 deformations and stresses in the soft tissues of the foot: A new approach in gait analysis. *J*
475 *Biomech* 2006;39:2673–89.
- 476 [28] Goske S, Erdemir A, Petre MT, Budhabhatti S, Cavanagh PR. Reduction of plantar heel
477 pressures: Insole design using finite element analysis. *J Biomech* 2006;39:2363–70.
- 478 [29] Gefen A. Plantar soft tissue loading under the medial metatarsals in the standing diabetic foot.
479 *Med Eng Phys* 2003;25:491–9.
- 480 [30] Luo G, Houston VL, Garbarini MA, Beattie AC, Thongpop C. Finite element analysis of heel
481 pad with insoles. *J Biomech* 2011;44:1559–65.
- 482 [31] Sacco ICN, Hamamoto AN, Tonicelli LMG, Watari R, Ortega NRS, Sartor CD. Abnormalities
483 of plantar pressure distribution in early, intermediate, and late stages of diabetic neuropathy.
484 *Gait Posture* 2014;40:570–4.

- 485 [32] García-Pérez J a, Pérez-Soriano P, Llana S, Martínez-Nova A, Sánchez-Zuriaga D. Effect of
486 overground vs treadmill running on plantar pressure: influence of fatigue. *Gait Posture*
487 2013;38:929–33.
- 488 [33] Verdejo R, Mills NJ. Heel-shoe interactions and the durability of EVA foam running-shoe
489 midsoles. *J Biomech* 2004;37:1379–86.
- 490 [34] Fontanella CG, Forestiero a, Carniel EL, Natali a N. Analysis of heel pad tissues mechanics at
491 the heel strike in bare and shod conditions. *Med Eng Phys* 2013;35:441–7.
- 492 [35] Cho J-R, Park S-B, Ryu S-H, Kim S-H, Lee S-B. Landing impact analysis of sports shoes
493 using 3-D coupled foot-shoe finite element model. *J Mech Sci Technol* 2009;23:2583–91.
- 494 [36] Pai S, Ledoux WR. The quasi-linear viscoelastic properties of diabetic and non-diabetic
495 plantar soft tissue. *Ann Biomed Eng* 2011;39:1517–27.
- 496 [37] Natali a. N, Fontanella CG, Carniel EL, Young JM. Biomechanical behaviour of heel pad
497 tissue experimental testing, constitutive formulation, and numerical modelling. *Proc Inst Mech*
498 *Eng Part H J Eng Med* 2011;225:449–59.
- 499 [38] Natali a N, Fontanella CG, Carniel EL. Constitutive formulation and analysis of heel pad
500 tissues mechanics. *Med Eng Phys* 2010;32:516–22.
- 501 [39] Uccioli L, Caselli A, Giacomozzi C, Macellari V, Giurato L, Lardieri L, et al. Pattern of
502 abnormal tangential forces in the diabetic neuropathic foot. *Clin Biomech* 2001;16:446–54.
- 503 [40] Yavuz M, Tajaddini A, Botek G, Davis BL. Temporal characteristics of plantar shear
504 distribution: relevance to diabetic patients. *J Biomech* 2008;41:556–9.

505

506

507

508

509

510

511

512

513

514

515

516 **Tables:**

517

518 Table 1: The maximum pressure reduction that was achieved for insole materials with $\alpha_{\text{foam}} = 4, 6$ and 8
 519 and for the cases of altered heel pad stiffness, thickness and loading. The respective optimum
 520 values of μ_{foam} are also shown in brackets for each one of these cases.

521

522

		Heel pad stiffness			Heel pad thickness			Heel pad loading		
		“Stiff”	Average	“Soft”	“Thick”	Average	“Thin”	240N	160N	80N
$\alpha_{\text{foam}}=4$	Max. pressure reduction (%)	31.6 (52kPa)	26.4 (52kPa)	27.9 (73kPa)	22.8 (52kPa)	26.4 (21kPa)	33.6 (52kPa)	29.2 (150kPa)	26.3 (116kPa)	26.4 (52kPa)
	Max. pressure reduction (%)	32.4 (52kPa)	26.5 (52kPa)	28.4 (52kPa)	23.1 (52kPa)	26.5 (52kPa)	33.8 (52kPa)	29.3 (150kPa)	26.1 (116kPa)	26.5 (52kPa)
	Max. pressure reduction (%)	31.8 (61kPa)	26.0 (52kPa)	27.5 (61kPa)	22.5 (52kPa)	26.0 (52kPa)	32.9 (52kPa)	29.1 (150kPa)	26.0 (116kPa)	26.0 (52kPa)

523

524

525

526

527

528

529

530

531

532

533

534

535

536 **Figure legends**

537 **Figure 1:** The ultrasound indentation device and a schematic representation of the procedure followed
538 to create the tissue's force/deformation curve.

539

540 **Figure 2:** (A) The frontal ultrasound image of the heel that was used for the reconstruction of the
541 geometry of the calcaneus. (B) Using Matlab the ultrasound image is divided by a series of line segments
542 with a relative distance of 2 mm. These lines are used as “search paths” to identify the transition points
543 between bone and soft tissue. When imported into ANSYS the coordinates of these key points are utilised
544 to create a polynomial line that outlines the calcaneus. (C) The geometry of the final FE model of the
545 indentation test.

546

547 **Figure 3:** The experimental force/deformation curve for the indentation test and the respective
548 numerical curve for the final best solution for the inverse engineering procedure.

549 **Figure 4:** (A) The FE model that was used for the estimation of plantar pressure and its application for
550 the cases of barefoot standing on a rigid surface (B) and barefoot standing on a 10mm thick sheet of an
551 insole material (C). The material properties of this insole material correspond to the PU foam used for
552 the validation of the model. Both pressure distributions (Pa) are calculated for a maximum load of 80N
553 and their peak values were used to calculate the pressure reduction that can be achieved by the PU foam.

554

555 **Figure 5:** A schematic representation of a loading scenario that closely matches the performed
556 simulations and was used for the validation of the subject-specific FE model.

557

558 **Figure 6:** The reduction of peak plantar pressure (A), the total energy absorbed during loading (B) and
559 the maximum deformation of the insole material (C) for insoles that have different mechanical
560 behaviour as defined by different μ_{foam} and α_{foam} values. The peak values of each graph are marked with
561 star.

562

563 **Figure 7:** The effect of different heel pad stiffness (A, B), thickness (C,D) and loading (E,F) to the
564 optimum cushioning properties of an insole material. For each one of these cases the reduction of peak
565 plantar pressure (%) and the total energy absorbed during loading (Nm) is presented for insoles that
566 have different stiffness. To improve clarity, the results presented in this figure correspond to insole
567 materials that have different μ_{foam} coefficients but the same α_{foam} coefficient (i.e. $\alpha_{\text{foam}} = 6$).

568

569

570

571

572

573

574

575

576

577

578

579 **Supplementary material captions**

580 **Suppl. Mat. 1:** A detailed description of the method that was used to inverse engineer the material
581 coefficients of the heel-pad.

582 **Suppl. Mat. 2:** The methodological approach for the calculation of the hyperelastic material coefficients of
583 commercially available PU foam.

584

585

586

587

588

589

590

591

592

593

594

595

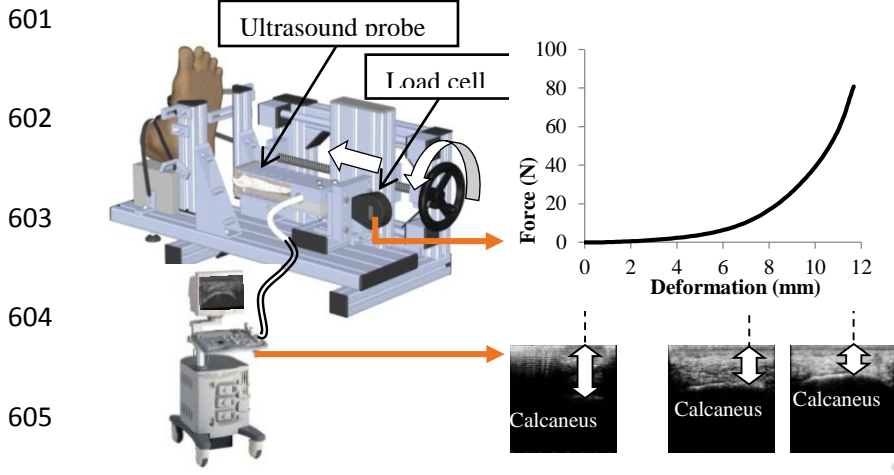
596

597

598

599 Figure 1

600



606

607

608

609

610

611

612

613

614

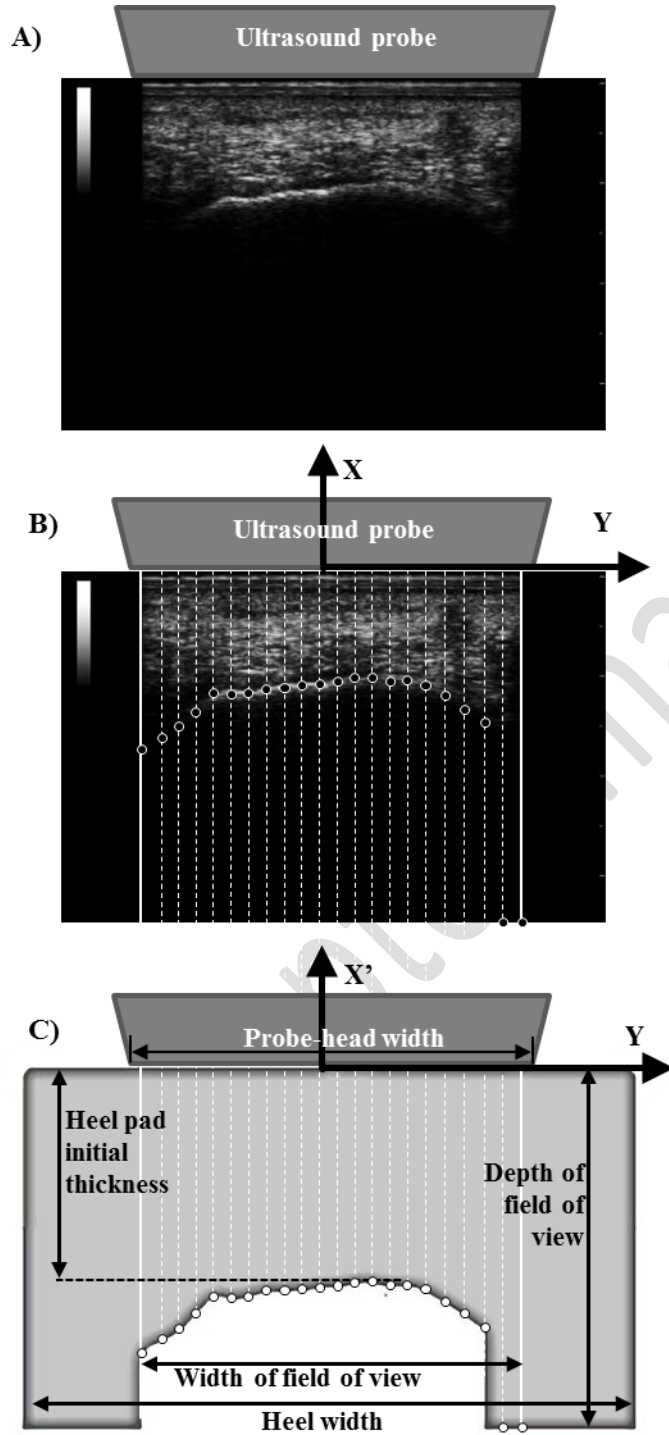
615

616

617

618 Figure 2

619



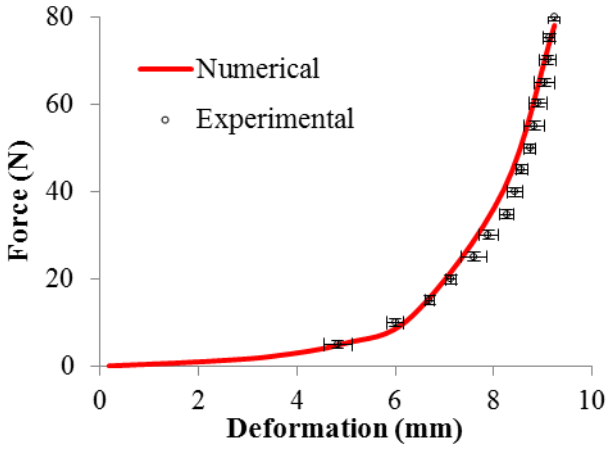
620

621

622

623 Figure 3

624



625

626

627

628

629

630

631

632

633

634

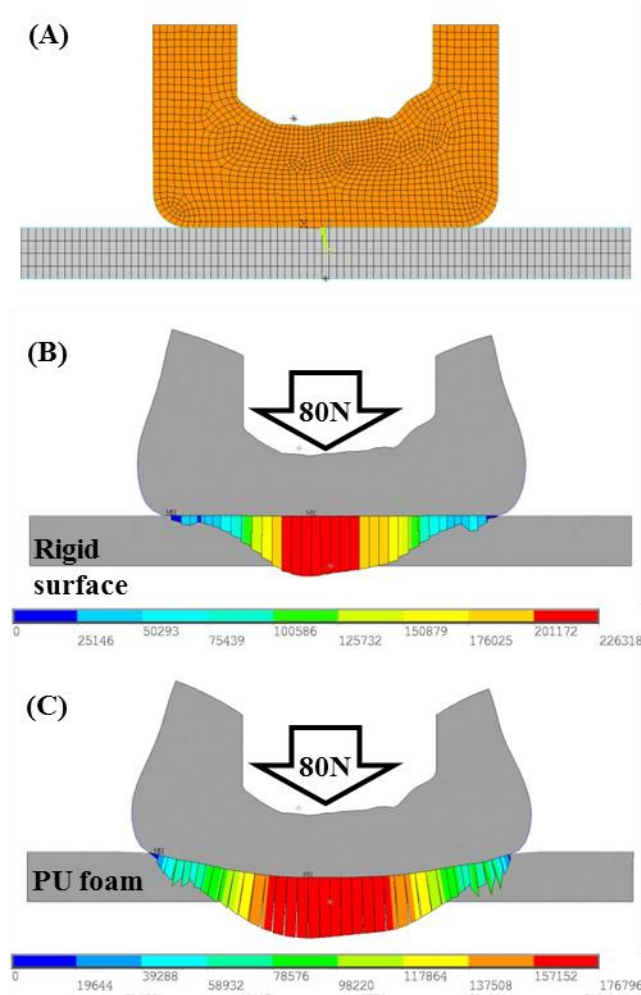
635

636

637

638 Figure 4

639



640

641

642

643

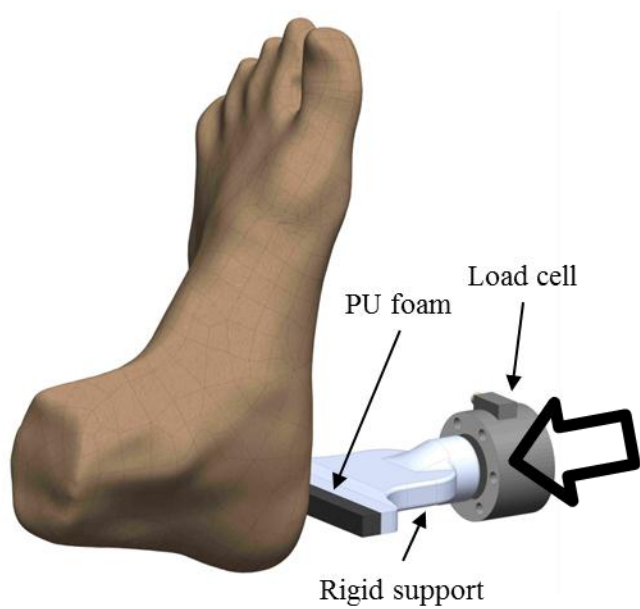
644

645

646

647 Figure 5

648



649

650

651

652

653

654

655

656

657

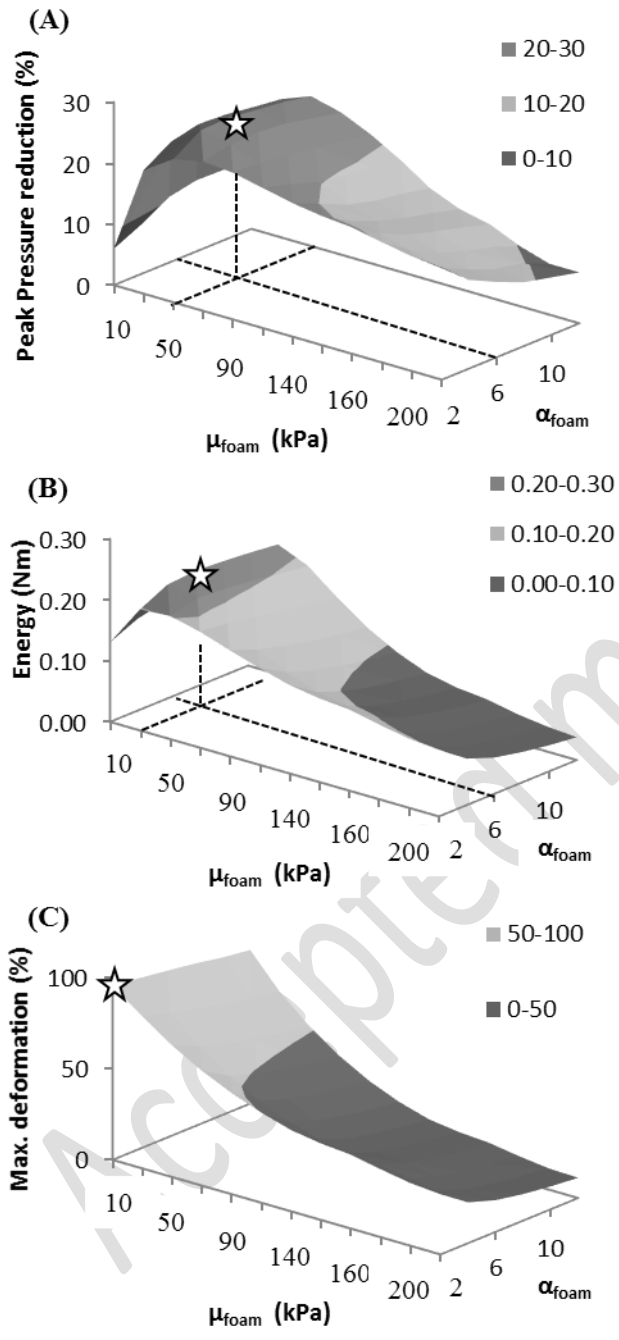
658

659

Accepted manuscript

660 Figure 6

661



662

663

664

665

